NANOSYSTEMS:
PHYSICS, CHEMISTRY, MATHEMATICS

Fedorova M., et al. *Nanosystems: Phys. Chem. Math.*, 2025, **16** (6), 785–790.
http://nanojournal.ifmo.ru
DOI 10.17586/2220-8054-2025-16-6-785-790

Original article

Multilevel physical unclonable function based on silver nanostructures randomly integrated into the crystalline silicon wafer

Maria Fedorova[1,a], Elena Petrova[1,b], Artem Larin[1,c], Martin Sandomirskii[1,d], Anna Ermina[2,e], Sergey Pavlov[2,f], Yuliya Zharova[2,g], Dmitry Permyakov[1,h], Vitaly Yaroshenko[1,i], Dmitry Zuev[1,j]

[1]School of Physics and Engineering, Faculty of Physics, ITMO University, St. Petersburg, Russia
[2]Ioffe Institute, 194021, St. Petersburg, Russia

[a]mariya.fedorova@metalab.ifmo.ru, [b]elena.petrova@metalab.ifmo.ru, [c]artem.larin@metalab.ifmo.ru, [d]m.sandomirskii@metalab.ifmo.ru, [e]annaermina@mail.ioffe.ru, [f]pavlov_sergey@mail.ioffe.ru, [g]piliouguina@mail.ioffe.ru, [h]d.permyakov@metalab.ifmo.ru, [i]v.yaroshenko@metalab.ifmo.ru, [j]d.zuev@metalab.ifmo.ru

Corresponding author: V. Yaroshenko, v.yaroshenko@metalab.ifmo.ru

ABSTRACT We present an optical physical unclonable function (PUF) based on silver nanostructures randomly formed on a crystalline silicon wafer through galvanic displacement and thermal annealing. The process produces nanostructures with stochastic spatial distribution and morphology, resulting in unpredictable nonlinear optical responses. The hybrid Ag–Si interface generates two independent signals: photoluminescence (PL) and second-harmonic generation (SHG). Spatial PL and SHG maps were binarized and analyzed using standard PUF metrics. SHG demonstrated higher entropy and more balanced bit distribution, making it the preferred encoding channel, while PL provides an additional verification layer. The fabrication method is scalable, lithography-free, and compatible with standard silicon processing.

KEYWORDS silver nanostructures, silicon, SHG, photoluminescence, physical unclonable function.

ACKNOWLEDGEMENTS Part of this work related to the photoluminescence measurements was supported by Russian Science Foundation project # 25-72-20030, https://rscf.ru/en/project/25-72-20030/ Part of this work related to the PUF labels creation and studies is supported by the Russian Science Foundation # 25-12-00310, https://rscf.ru/en/project/25-12-00310/

FOR CITATION Fedorova M., Petrova E., Larin A., Sandomirskii M., Ermina A., Pavlov S., Zharova Y., Permyakov D., Yaroshenko V., Zuev D. Multilevel physical unclonable function based on silver nanostructures randomly integrated into the crystalline silicon wafer. *Nanosystems: Phys. Chem. Math.*, 2025, **16** (6), 785–790.

1. Introduction

The modern global economy faces a growing threat from counterfeit goods, which inflict significant financial losses on manufacturers and pose serious risks to consumers, particularly in critical sectors such as pharmaceuticals [1, 2]. Conventional protection methods like holograms and barcodes are vulnerable to copying, as they are created using deterministic algorithms. A promising solution to this problem lies in Physical Unclonable Functions (PUFs), which leverage stochastic processes at their core to ensure the uniqueness and unpredictability of each item [3–5].

PUFs are hardware-based cryptographic primitives that exploit the inherent randomness of their physical structure to generate unique challenge-response pairs. For anti-counterfeiting, optical PUFs are of particular interest due to their high information capacity and resistance to tampering. However, current manufacturing techniques for strong optical PUFs are often incompatible with existing production lines [6] and/or vulnerable to sophisticated machine learning attacks. Furthermore, the long-term security of many PUF designs is threatened by their reliance on microscopic features, which are becoming increasingly susceptible to manipulation as nanoscale technologies advance.

The logical evolution of PUFs involves a shift to nanoscale critical features, which would drastically enhance their resistance to cloning [7,8]. Yet, this transition introduces fundamental readout challenges, requiring sub-diffraction spatial imaging techniques and robustness against higher noise levels. Consequently, a key challenge is the development of PUFs that combine nanoscale complexity with fabrication simplicity and reliable readout protocols. Multi-level security system, that combines different optical responses [9, 10] add complexity into label design, represents a promising direction for creating authentication systems.

Here, we introduce a novel, high-security PUF label based on a stochastic assembly of silver nanoparticles on a silicon wafer. The unique cryptographic identity of each label is derived from its inherent morphological randomness, which

manifests as a non-linear optical response, specifically through second harmonic generation (SHG) and photoluminescence (PL). We detail a scalable fabrication approach for these structures and thoroughly characterize their morphology and optical properties. Furthermore, we demonstrate their practical application as robust PUF label and evaluating their encoding capacity, showcasing their potential for anti-counterfeiting solutions.

2. Results

2.1. Fabrication

Commercial boron-doped (p-type), single-crystal silicon (c-Si) wafers with a thickness of 500 μm and (100) crystallographic orientation, grown by the Czochralski method and chemically dynamically polished on one side, were purchased from Telecom-STV Company Limited (Zelenograd, Russia). The wafers had a resistivity of 10 Ω cm, corresponding to a carrier concentration of approximately 1.4×10^{16} cm^{-3}. For convenience, the wafers were diced into 1×2 cm^2 samples. Prior to experiments, the c-Si samples underwent wet chemical cleaning based on the RCA procedure to remove organic and ionic contaminants. Milli-Q deionized water and fluoroplastic dishes were used throughout the experiment. Argentum nanoparticles (AgNPs) were synthesized on the surface of c-Si wafers (see Fig. 1a) via a galvanic displacement reaction (GDR) using an aqueous solution of 0.02 M $AgNO_3$:5 M HF mixed at volume ratio of 1:1 at room temperature. The c-Si wafer was immersed in the solution for 30 s, then rinsed with deionized water for 30 s, and subsequently dried with compressed air to prevent streak formation on the sample surface. In the GDR process, the reduction of Ag^+ on the c-Si substrate is driven by the substrate itself upon immersion in the solution. In this redox system, c-Si, having a lower electrochemical potential (-0.857 V vs. the standard hydrogen electrode (SHE)), is displaced by Ag^+ ions from the solution, which have a higher potential (0.8 V vs. SHE) [11]. The GDR in an HF-containing solution involves simultaneous anodic and cathodic processes occurring on the c-Si surface, with charge exchange facilitated through the substrate. Fluoride ions play a critical role by dissolving oxidized silicon in the form of silicon hexafluoride (SiF_6^{2-}), thereby preventing the formation of a layer of native silicon oxide (SiO_2). This maintains access to a fresh c-Si surface and sustains the reaction. Thus, the overall ionic redox reaction can be written as follows [11]:

$$4\mathrm{Ag}^+(aq) + \mathrm{Si}_0(s) + 6\mathrm{F}^-(aq) = 4\mathrm{Ag}_0(s) + \mathrm{SiF}_6^{2-}(aq) \tag{1}$$

where aq and s denote the aqueous and solid phases, respectively. The ionic reaction (1) can be interpreted as a short-circuited galvanic cell composed of two electrodes: Cathodic half-reaction:

$$\mathrm{Ag}^+(aq) + e^- = 4\mathrm{Ag}_0(s) \tag{2}$$

Anodic half-reaction:

$$\mathrm{Si}_0(s) + 6\mathrm{F}^-(aq) = \mathrm{SiF}_6^{2-}(aq) + 4e^- \tag{3}$$

where e^- denotes an electron.

Following the galvanic deposition of AgNPs onto c-Si, the samples underwent high-temperature annealing at 1000°C in H_2O atmosphere for 5 min. The annealing process was carried out in a three-phase electric muffle furnace equipped with six silicon carbide heating elements. The furnace temperature was monitored and regulated using a thermocouple positioned in the working zone and controlled via an electronic temperature control unit. During annealing, the experimental samples were placed on a flat quartz support, which was positioned at the long end of a quartz L-shaped tube. The short end of the tube was filled with boiling water to generate water vapor. The entire assembly was then inserted into the furnace's working area. Upon completion of the annealing time, the quartz tube was withdrawn from the furnace, and the samples were allowed to cool to room temperature under ambient conditions. This process yielded SiO_2/AgNPs/c-Si(100) composite structures. The thermally grown SiO_2 layer was selectively removed by immersion in a 1:1 HF:H_2O solution for 5 min(see Fig. 1a). To obtain pits in c-Si, silver was dissolved in boiling HNO_3 for 3 min(see Figs. 1b,c).

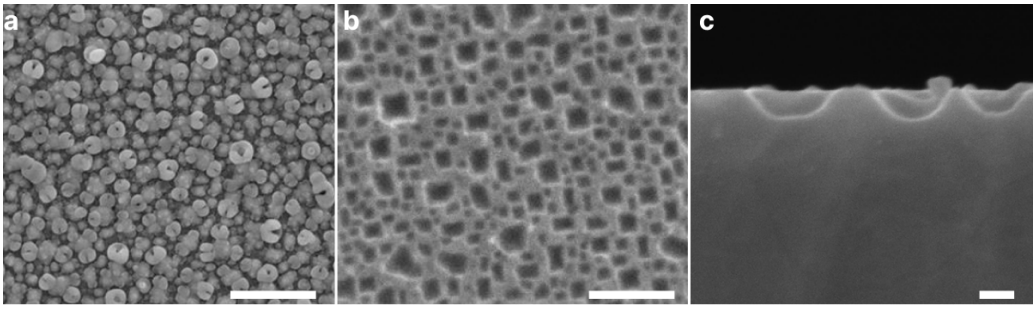

FIG. 1. Morphology of the nanostructures shown by SEM images. (a) Silver nanostructures on the silicon surface. (b-c) c-Si wafer after process of removal SiO_2/AgNPs structures. Top and side view respectively. Scale bar for (a) and (b) corresponds to 1 um, (c) – 100 nm

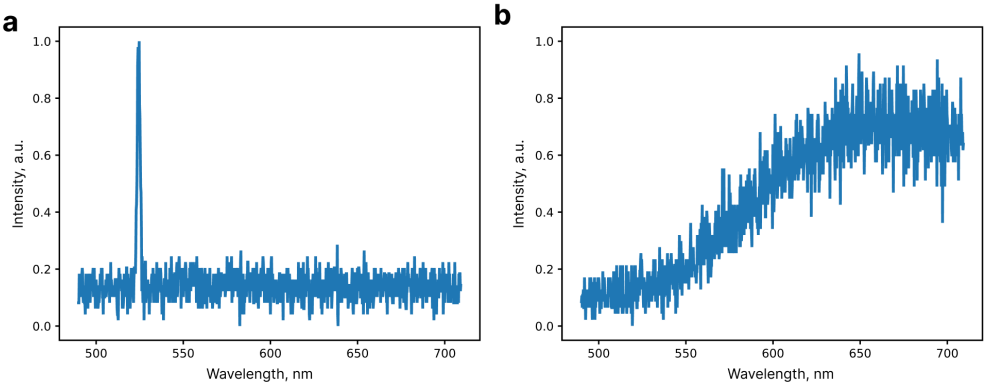

FIG. 2. SHG and PL spectra from nanostructures located at different points of the sample. (a) The spectrum of the structure shows only SHG. (b) The spectrum of the structure shows only PL

2.2. Optical characterization

In the previous section, we described in detail the fabrication process used to synthesize AgNPs embedded in the surface of the crystalline silicon wafer. Due to the stochastic thermodynamic nature of the GDR and annealing processes central to our approach, the AgNPs formed on the resulting samples exhibited random spatial distributions, sizes, and shapes (see Fig. 1a).

Next, we investigated the nonlinear optical properties of the fabricated samples. For this purpose, we employed an ultrafast Yb^{3+} laser system (TeMa, Avesta Project) with a central wavelength of 1050 nm, pulse duration of 150 fs, and repetition rate of 80 MHz. The laser beam was attenuated to 5 mW and focused onto the sample surface using a 100x / 0.7 NA Mitutoyo MPlan APO NIR objective in reflection configuration with dichoic mirror Thorlabs DMSP900. The resulting optical signal from the samples was collected by the same objective and projected onto a charge-coupled device (Andor DU420A-OE 325) placed in a Horiba LabRam HR spectrometer equipped with a 150 lines mm^{-1} diffraction grating.

Fig. 2 shows spectra of second-harmonic generation (SHG) and photoluminescence (PL) recorded from one of the fabricated samples under the described experimental conditions. It can be clearly seen that all observed nonlinear responses arise exclusively in the presence of AgNPs (see Figs. 1,3). This observation is consistent with the fact that bulk silicon possesses an extremely low quantum yield due to its indirect bandgap [12]. In contrast, the formation of metal-semiconductor (Ag–Si) interfaces provides an effective mechanism for enhancing the nonlinear optical response of silicon. Indeed, the metallic component significantly increases optical absorption in the system and facilitates the injection of hot electrons into the active material [13]. This, in turn, leads to a high concentration of electrons in the Si conduction band, improving the radiative recombination efficiency through enhanced Auger recombination [14]. Simultaneously, the SHG signal can be attributed to the local symmetry breaking occurring at the same metal-semiconductor interfaces [15, 16].

Interestingly, analysis of the optical maps reveals that some AgNPs help to generate PL(see Fig. 2b), while others help to produce primarily SHG(see Fig. 2a). We attribute this effect to the possible formation of a thin silver sulfide shell around certain nanoparticles during fabrication [17]. Depending on its thickness and uniformity, this sulfide layer can act as an additional energy barrier at the Ag–Si interface, suppressing hot electron injection into the silicon and thereby reducing PL efficiency (while leaving SHG less affected). Nevertheless, we assume that the formation of such a sulfide shell is a matter of chance, which makes the observed "switching" behavior between PL- and SHG-dominated regions essentially random.

2.3. Designing a PUF label

Here we propose a hybrid optical PUF label based on silicon – silver nanostructures that simultaneously exhibit PL and SHG. The stochastic spatial distribution of nanostructures and there "switching" behavior results from the fabrication process and cannot be deterministically reproduced, which forms the foundation of the PUF design. As explained above these two optical responses arise from different physical mechanisms. Thus, the label naturally offers two independent optical response channels, enabling multi-layer authentication and increased resistance to copping.

To evaluate whether PL and SHG encode independent information, we computed the Pearson correlation coefficient between the binary response patterns extracted from the PL and SHG maps. The Pearson correlation coefficient quantifies the degree of linear dependence between two datasets, ranging from -1 (complete negative dependence) to $+1$ (complete positive dependence), with 0 indicating no correlation. In the context of physically unclonable functions, low correlation is desired, as it indicates that different optical responses do not contain same information and therefore contribute additional security entropy. The coefficient was calculated based on binarized spatial patterns, where each bit corresponds to the presence or absence of an optical signal exceeding noise. The binarization process is shown in Fig. 3.

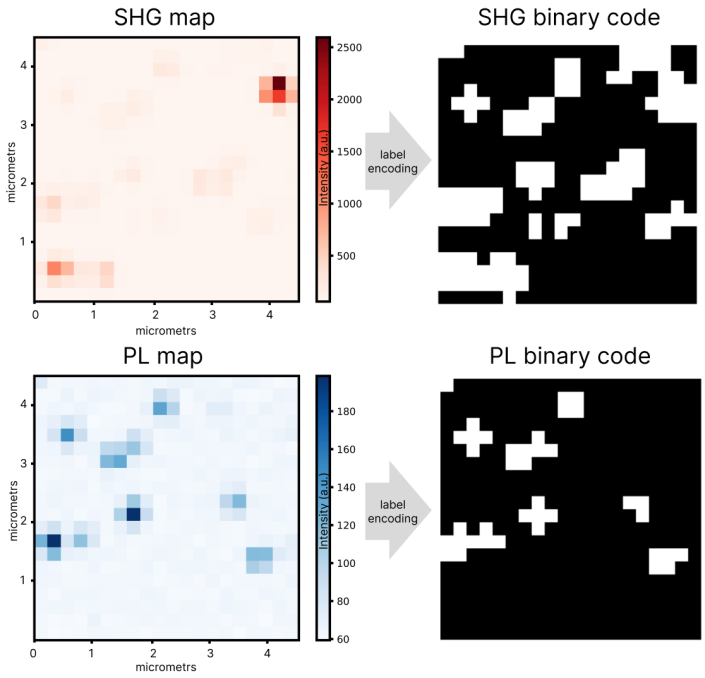

FIG. 3. The encoding scheme of the label. Demonstration of the process of converting SHG and PL intensity maps into binary code

The resulting Pearson correlation coefficient between the PL-derived and SHG-derived patterns was 0.48, indicating only moderate correlation and confirming that SHG does not replicate the PL-encoded information. For comparison, we also analyzed the correlation between PL intensity maps at two wavelengths (650 nm and 700 nm) and obtained a value of 0.86, which is significantly closer to 1. This high correlation is expected because both datasets originate from the same PL mechanism. In contrast, the much lower correlation between PL and SHG demonstrates that the nonlinear optical channel adds an additional, statistically independent layer of cryptographic entropy. These results confirm that combining PL and SHG in a single nanostructured label enables a dual-level optical PUF architecture with enhanced resistance to duplication.

The encoding capacity (EC) of the proposed dual-channel PUF was estimated from the number of independent bits encoded in the PL and SHG patterns. Each label consists of a 20×20 pixel grid (400 cells), and each cell provides two independent binary responses (PL and SHG). Therefore, the total encoding capacity of a single PUF label is:

$$EC = 2^{2\times 20\times 20} \approx 10^{240}. \tag{4}$$

Encoding capacity shows us amount of possible unique challenge-response pairs. Calculated value exceeds the encoding capacity typically reported for rudimentary PUFs and is comparable to values demonstrated in recent high-capacity implementations [18].

In addition to the high encoding capacity, the performance of the generated binary patterns was evaluated using three widely adopted PUF quality metrics [19]: bit uniformity, uniqueness, and entropy, calculated separately for the SHG-based and PL-based responses.

Bit uniformity (BU) quantifies the balance between 0 and 1 in the generated response, with an ideal value of 0.5 indicating the absence of bias toward either state. Bit uniformity can be calculated with followed formula [20]:

$$BU = \frac{1}{t}\sum_{n=1}^{t} K_n, \tag{5}$$

where K_n is the bit number n in the binary code.

For the SHG-derived patterns, bit uniformity was 0.1, while for PL it was 0.05. Although these values deviate from the ideal symmetric distribution, such behavior is typical for physically generated binary responses where digitization results from localized variations of optical intensity. This is due to the large amount of “empty” space, which gives one zero response.

Uniqueness (U) evaluates the average Hamming distance between different responses and reflects how distinguishable binary patterns are when obtained from different spatial regions. For calculations, the following formula was used [21]:

$$U = \frac{2}{k(k-1)} \sum_{i=1}^{k-1} \sum_{j=i+1}^{k} \frac{HD(R_i, R_j)}{R}, \tag{6}$$

where R_i and R_j represent the responses from the labels i and j. The number of labels is k, and HD denotes the Hamming distance. SHG-based responses demonstrated a uniqueness of 0.2, whereas PL yielded 0.1.

Finally, we calculated entropy (E) It shows the level of unpredictability in the binary data. Higher entropy corresponds to stronger resistance against brute-force or statistical prediction attacks. The entropy values obtained for SHG and PL responses were 0.5 and 0.3, respectively. The following formula was used [22]:

$$E = -[p \log_2 p + (1-p) \log_2 (1-p)], \tag{7}$$

where p is the probability of 1 in binary code.

Analyzing these parameters, we can conclude that SHG-derived patterns show better characteristics for generating random bit sequences than PL-derived ones. This is due to the fact that SHG responses are present in more structures on the label surface than the photoluminescence response.

3. Conclusion

We demonstrated a dual-channel optical PUF based on randomly formed Ag nanostructures on a silicon wafer. This structures are able to produce PL and SHG signals, which can be independently detected and converted into binary patterns. Analysis of the obtained patterns shows that PL- and SHG-based responses encode different information. Evaluation of bit uniformity, uniqueness and entropy confirms that SHG provides a more balanced and informative binary output and is therefore more suitable as the primary channel for encoding, while PL can serve as an additional layer of verification. The presented fabrication approach is simple and scalable. All steps – galvanic displacement of silver and thermal annealing and selective etching – rely on well-established wafer-level methods that do not require lithography or specialized equipment. The process can be carried out on commercially available silicon wafers and repeated across large areas without additional patterning. Since randomness is introduced naturally during metal deposition and interface formation, no external randomness source or design optimization is needed. These features make the method feasible for integration into existing semiconductor production workflows and suitable for low-cost manufacturing of optical PUF labels.

References

[1] Kikerkova I., Toshevska Trpchevska K., Kikerkov I. Threats of trade in counterfeit pharmaceutical products. *Horizons - International Scientific Journal*, 2022, **31**(2), P. 7–23.

[2] Ofori-Parku S. Fighting the global counterfeit medicines challenge: A consumer-facing communication strategy in the US is an imperative. *Journal of Global Health*, 2022, **12**.

[3] Ali S., Kershaw S., Faisal M., Halak B., Abdelazim N. Illuminating advances in materials: optical physical unclonable functions for security applications. *Advanced Optical Materials*, 2025, **13**(29), P. e01564.

[4] Klausen M., Zhang J., Stevens M. Designing physical unclonable functions from optically active materials. *Advanced Materials*, 2025, P. 2502059.

[5] Mishra P., Manna A., Ray N. Advances in semiconductor quantum dot-based physical unclonable functions for enhanced security applications. *Nanoscale*, 2025, **17**, P. 20865–20879.

[6] Gandla S., Moon C., Leem J., Yoon J., Yun H., Kim M., Kim D., Lee S., Yao Y., Alexandropoulos D., Song Y., Yoon D., Park W., Kim Y., Kim S. Multiplex optical unclonable functions: advances and perspectives in optics and photonics for hardware security. *ACS Nano*, 2025, **19**(30), P. 27033–27074.

[7] Junhyuk A., Taesung P., Taewoo K., Seong-Gyun I., Hanseok S., Bong-Hoon K., Seok Joon K., Soong Ju O. Nanoseed-based physically unclonable function for on-demand encryption. *Science Advances*, 2025, **11**(17), P. eadt7527.

[8] Kim J., Jeon S., In J., Nam S., Jin H., Han K., Yang G., Choi H., Kim K., Shin J., Son S., Kwon S., Kim B., Kim S. Nanoscale physical unclonable function labels based on block copolymer self-assembly. *Nature Electronics*, 2022, **5**(7), P. 433–442.

[9] Guo H., Qin Y., Wang Z., Ma Y., Wen H., Li Z., Ma Z., Li X., Tang J., Liu J. Multilevel encoding physically unclonable functions based on the multispecies structure in diamonds. *Advanced Functional Materials*, 2024, **34**(15), P. 2304648.

[10] Yang J., Li Y., Ju D., Liang F., Liu S., Song F. Bio-replicated multilevel physical unclonable fluorescent glass labels enabled by artificial intelligence authentication. *Chemical Engineering Journal*, 2025, **510**, P. 161538.

[11] Carraro C., Maboudian R., Magagnin L. Metallization and nanostructuring of semiconductor surfaces by galvanic displacement processes. *Surface Science Reports*, 2007, **62**(12), P. 499–525.

[12] Priolo F., Gregorkiewicz T., Galli M., Krauss T. Silicon nanostructures for photonics and photovoltaics. *Nature Nanotechnology*, 2014, **9**(1), P. 19–32.

[13] Gurbatov S., Puzikov V., Storozhenko D., Modin E., Mitsai E., Cherepakhin A., Shevlyagin A., Gerasimenko A., Kulinich S., Kuchmizhak A. Multigram-Scale production of hybrid Au-Si annomaterial by laser ablation in liquid (LAL) for temperature-feedback optical nanosensing, light-to-heat conversion, and anticounterfeit labeling. *ACS Appl. Mater. Interfaces*, 2023, **15**(2), P. 3336–3347.

[14] Makarov S., Sinev I., Milichko V., Komissarenko F., Zuev D., Ushakova E., Mukhin I., Yu Y., Kuznetsov A., Belov P., Iorsh I., Poddubny A., Samusev A., Kivshar Yu. Nanoscale generation of white light for ultrabroadband nanospectroscopy. *Nano Lett.*, 2018, **18**(1), P. 535–539.

[15] Makarov S., Petrov M., Zywietz U., Milichko V., Zuev D., Lopanitsyna N., Kuksin A., Mukhin I., Zograf G., Ubyivovk E., Smirnova D., Starikov S., Chichkov B., Kivshar Yu. Efficient second-harmonic generation in nanocrystalline silicon nanoparticles. *Nano Lett.*, 2017, **17**(5), P. 3047–3053.

[16] Sandomirskii M., Petrova E., Kustov P., Chizhov L., Larin A., Bruyère S., Yaroshenko V., Ageev E., Belov P., Zuev D. Spectral physical unclonable functions: downscaling randomness with multi-resonant hybrid particles. *Nature Communications*, 2025, **16**(1), P. 5097.

[17] McMahon M., Lopez R., Meyer III H., Feldman L., Haglund Jr R. Rapid tarnishing of silver nanoparticles in ambient laboratory air. *Applied Physics B*, 2005, **80**(7), P. 915–921.
[18] Wang K., Shi J., Lai W., He Q., Xu J., Ni Z., Liu X., Pi X., Yang D. All-silicon multidimensionally-encoded optical physical unclonable functions for integrated circuit anti-counterfeiting. *Nature Communications*, 2024, **15**(1), P. 3203.
[19] Lin X., Li Q., Tang Y., Chen Z., Chen R., Sun Y., Lin W., Yi G., Li Q. Physical unclonable functions with hyperspectral imaging system for ultrafast storage and authentication enabled by random structural color domains. *Advanced Science*, 2024, **11**(31), P. 2401983.
[20] Jiao F., Lin C., Dong L., Wu Y., Xiao Y., Zhang Z., Sun J., Zhao W., Li S., Yang X., Ni P., Wang L., Shan C. Traceable optical physical unclonable functions based on germanium vacancy in diamonds. *ACS Applied Materials & Interfaces*, 2024, **16**(33), P. 44328-44339.
[21] Balijabudda V., Acharya K., Chakraborty R., Chakrabarti I. Theoretical enumeration of deployable single-output strong PUF instances based on uniformity and uniqueness constraints. Proceeding of "19th International Conference, ICISS 2023", Raipur, India, 16-20 December 2023, Springer Nature Switzerland, P. 77–87.
[22] Gandla S., Moon C., Leem J., Yoon J., Yun H., Kim M., Kim D., Lee S., Yao Y., Alexandropoulos D., Song Y., Yoon D., Park W., Kim Y., Kim S. Multiplex optical unclonable functions: advances and perspectives in optics and photonics for hardware security. *ACS Nano*, 2025, **19**(30), P. 27033–27074.

Submitted 7 November 2025; revised 19 November 2025; accepted 20 November 2025

Information about the authors:

Maria Fedorova – School of Physics and Engineering, Faculty of Physics, ITMO University, St-Petersburg, Russia; ORCID 0009-0002-5213-5217; mariya.fedorova@metalab.ifmo.ru

Elena Petrova – School of Physics and Engineering, Faculty of Physics, ITMO University, St-Petersburg, Russia; ORCID 0000-0003-1435-0274; elena.petrova@metalab.ifmo.ru

Artem Larin – School of Physics and Engineering, Faculty of Physics, ITMO University, St-Petersburg, Russia; ORCID 0000-0002-8609-9851; artem.larin@metalab.ifmo.ru

Martin Sandomirskii – School of Physics and Engineering, Faculty of Physics, ITMO University, St-Petersburg, Russia; ORCID 0000-0002-3115-1739; m.sandomirskii@metalab.ifmo.ru

Anna Ermina – Ioffe Institute, 194021, St. Petersburg, Russia; ORCID 0000-0001-9010-7482; annaermina@mail.ioffe.ru

Sergey Pavlov – Ioffe Institute, 194021, St. Petersburg, Russia; ORCID 0000-0001-9589-8017; pavlov_sergey@mail.ioffe.ru

Yuliya Zharova – Ioffe Institute, 194021, St. Petersburg, Russia; ORCID 0000-0001-7002-5084; piliouguina@mail.ioffe.ru

Dmitry Permyakov – School of Physics and Engineering, Faculty of Physics, ITMO University, St-Petersburg, Russia; ORCID 0000-0003-2708-9140; d.permyakov@metalab.ifmo.ru

Vitaly Yaroshenko – School of Physics and Engineering, Faculty of Physics, ITMO University, St-Petersburg, Russia; ORCID 0000-0003-2034-4962; v.yaroshenko@metalab.ifmo.ru

Dmitry Zuev – School of Physics and Engineering, Faculty of Physics, ITMO University, St-Petersburg, Russia; ORCID 0000-0001-9157-5683; d.zuev@metalab.ifmo.ru

Conflict of interest: the authors declare no conflict of interest.